Pergamon

Int. J. Heat Mass Transfer. Vol. 38, No. 15, pp. 2905–2914, 1995

0017–9310/95 $9.50+0.00

0017–9310(95)00081–X

Transport phenomena of developing laminar mixed convection heat and mass transfer in inclined rectangular ducts

WEI-MON YAN

Department of Mechanical Engineering, Hua Fan College of Humanities and Technology, Shih Ting, Taipei, Taiwan 22305, Republic of China

(*Received* 16 *June* 1994)

Abstract—The developing laminar mixed convection heat and mass transfer in inclined rectangular ducts has been studied numerically, with six independent parameters: Prandtl number Pr, mixed convection parameter Ω, modified Rayleigh number Ra^*, buoyancy ratio N, Schmidt number Sc and aspect ratio γ. Typical developments of velocity, temperature and concentration profiles are shown to include the limiting cases of horizontal and vertical rectangular ducts. Local friction factor, Nusselt number and Sherwood number are presented for species diffusion of interest in air ($Pr = 0.7$) over a Schmidt number range of 0.2–2.0. The results show that the $Nu(Sh)$ is charcterized by a decay near the inlet due to the entrance effect; but the decay is attenuated by the onset of buoyancy-driven secondary flows. The Nu (Sh) falls asymptotically to the value of Graetz problem when the temperature (concentration) profile becomes fully developed. The $fRe/(fRe)_0$, Nu and Sh are enhanced as the buoyancy force from species diffusion assists the thermal buoyancy force.

INTRODUCTION

Combined heat and mass transfer occurs due to the existence of temperature and concentration variations in nature and in many industrial applications. Mixed convection heat transfer influenced by thermal buoyancy has received much attention, but the effects of combined thermal and solutal buoyancies on mixed convection heat and mass transfer in a duct have not been widely studied. However, they are encountered in many practical situations, such as in the chemical distillatory processes, the design of heat exchangers, solar energy collectors and thermo-protection systems. For vertical ducts, the gravity force acts in the main flow direction, and there will be no secondary flow in the cross section. For horizontal ducts, the combined buoyancy forces are normal to the main flow direction and they induce secondary flows in the cross plane. For inclined ducts, however, buoyancy forces act in both main flow and the cross-stream directions.

Numerical and experimental studies of fully-developed mixed convection heat transfer are included in refs. [1, 2] for horizontal ducts and in refs. [3–6] for inclined ducts. Abdelmeguid and Spalding [7] have presented numerical predictions of fully-developed turbulent flow and heat transfer in uniformly heated, inclined tubes. However, the assumed fully-developed flow can only be established if the duct is very long. The detailed numerical studies on developing laminar mixed convection heat transfer have been studied in horizontal ducts [8–14] and in a vertical rectangular duct [15]. Abou-Ellail and Morcos [16] and Morcos and Abou-Ellail [17] presented a numerical solution for mixed convection heat transfer in the entrance region of inclined rectangular ducts. Photographs of developing secondary flow patterns in the thermal entrance region of inclined tubes for laminar mixed convection flow were presented by Cheng and Yuen [18]. Morcos *et al.* [19] performed an experimental study on laminar mixed convection heat transfer in the entrance region of inclined rectangular ducts. In ref. [19], an aluminum rectangular channel was used as a test section. Therefore, the wall conduction effect plays an important role in their studies. A numerical study of combined forced and free convection for laminar flow in the entrance region of isothermal, inclined tubes has been carried out by Choudhury and Patankar [20]. Their results revealed that the buoyancy effects have a considerable influence on the fluid flow and heat transfer characteristics of the development flow.

As far as mixed convection heat and mass transfer are concerned, Santarelli and Foraboschi [21] investigated the buoyancy effects of thermal and mass diffusion on laminar forced convection flow undergoing a chemical reaction. Yan [22, 23] studied the laminar mixed convection heat and mass transfer in a vertical two-dimensional duct, and found that the combined buoyancy forces of thermal and solutal diffusion have considerable effects on laminar forced convection heat and mass transfer. Recently, Lin *et*

NOMENCLATURE

A cross-sectional area of a horizontal rectangular duct [m^2]
a, b width and height of a rectangular duct, respectively [m]
c, C dimensional and dimensionless species concentration, respectively
D mass diffusivity
D_e equivalent hydraulic diameter, $4A/S$
f friction factor, $2\bar{\tau}_w/(\rho w_0^2)$
g gravitational acceleration [m s^{-2}]
Gr Grashof number, $g\beta(T_w - T_0)D_e^3/\nu^2$
$\bar{h}$ average heat transfer coefficient [W m^{-2} K^{-1}]
$\bar{h}_m$ average mass transfer coefficient
I, J number of finite difference divisions in X and Y directions, respectively
k thermal conductivity [W m^{-1} K^{-1}]
m mth iteration
N buoyancy ratio, $\beta^*(c_w - c_0)/[\beta(T_w - T_0)]$
n outward normal direction to the wall
Nu local Nusselt number, $\bar{h}D_e/k$
$\bar{p}$ cross-sectional mean pressure [kPa]
$\bar{P}$ dimensionless cross-sectional mean pressure
P' perturbation term about the mean pressure $\bar{P}$
Pr Prandtl number, ν/α
Ra Rayleigh number, $Pr\,Gr$
Ra^* modified Rayleigh number, $Ra\cos\delta$
Re Reynolds number, $w_0 D_e/\nu$
S circumference of cross section [m]
Sc Schmidt number, ν/D
Sh Sherwood number, $\bar{h}_m D_e/D$
T temperature [K]
T_0 inlet temperature [K]
T_w wall temperature
U, V, W dimensionless velocity components in X-, Y- and Z-directions, respectively
w_0 inlet axial velocity [m s^{-1}]
x, y, z rectangular coordinate [m]
X, Y, Z dimensionless rectangular coordinate, $X = x/D_e$, $Y = y/D_e$, $Z = z/(Re\,D_e)$
Z^* dimensionless z-direction coordinate, $z/(Pr\,Re\,D_e) = Z/Pr$.

Greek symbols

α thermal diffusivity [m^2 s^{-1}]
β coefficient of thermal expansion [K^{-1}]
β^* coefficient of concentration expansion
δ duct inclination angle
γ aspect ratio of a rectangular duct, a/b
θ dimensionless temperature, $(T - T_0)/(T_w - T_0)$
ν kinematic viscosity [m^2 s^{-1}]
ξ dimensionless vorticity in axial direction
ρ density [kg m^{-3}]
Ω mixed convection parameter, $(Ra/Re)\sin\delta$.

Subscripts

b bulk fluid quantity
0 value at inlet or fully-developed condition
w value at wall.

Superscripts

$^-$ average value.

al. [24] performed a numerical analysis on laminar mixed convection heat and mass transfer in a horizontal square duct.

It is noted in the above reviews that studies of developing mixed convection heat and mass transfer in inclined rectangular ducts have not received sufficient attention. This motivates the present investigation to examine the effects of combined buoyancy forces of thermal and solutal diffusion on laminar forced convection in inclined rectangular ducts.

ANALYSIS

Consideration is given to a steady laminar upward flow in the entrance region of a rectangular duct inclined at angle δ to the horizontal, as shown in Fig. 1. The fluid enters the channel with a uniform velocity w_0 and a constant inlet temperature T_0 and concentration c_0. The duct walls are subjected to a constant temperature T_w and concentration c_w. The problem is to analyze the heat and mass transfer for simultaneously developing laminar flow with combined buoyancy effects of thermal and solutal diffusion in inclined rectangular ducts. Because of the symmetry inherent in the problem, the calculations can be restricted to a solution domain that comprises one-half of the inclined rectangular duct as shown in Fig. 1, u, v and w being the velocity components in the x, y and z directions, respectively.

The flow is assumed to be steady and have constant thermophysical properties, except the buoyancy terms in the y- and z-direction momentum equations. As shown in ref. [25], the axial diffusion terms in the governing equations are negligible when the Peclet number is greater than 100. The buoyancy force resulting from the concentration difference may assist or

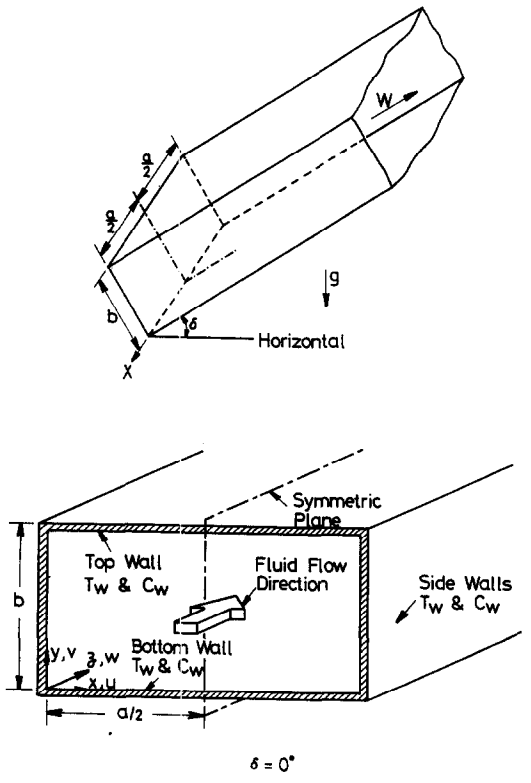

Fig. 1. Physical configuration and coordinate system.

oppose the buoyancy force from the temperature variation in the fluid. The axial and cross-sectional pressure gradients may be decoupled by making the usual parabolic assumption [26]. A modified pressure $p(x, y, z)$ can be defined as

$$p(x,y,z) = \bar{p}(z) + p'(x,y) \tag{1}$$

where $\bar{p}(z)$ is the pressure averaged over the cross section at each axial location, and $p'(x, y)$ is the pressure variation in the xy plane, which derives the secondary flow.

Introducing the following dimensionless independent and dependent variables:

$$\begin{aligned}
&X = x/D_e && Y = y/D_e \\
&Z = z/(Re\,D_e) && Z^* = Z/Pr \\
&U = uD_e/\nu && V = vD_e/\nu \\
&W = w/w_0 && \bar{P} = \bar{p}/(\rho_0 w^2) \\
&P' = p'/(\rho_0 \nu^2/D_e^2) && \theta = (T-T_0)/(T_w-T_0) \\
&C = (c-c_0)/(c_w-c_0) && Gr = g\beta(T_w-T_0)D_e^3/\nu^2 \\
&Ra = Pr\,Gr && N = \beta^*(c_w-c_0)/[\beta(T_w-T_0)] \\
&Ra^* = Ra\cdot\cos\delta && \Omega = (Ra/Re)\sin\delta \\
&Pr = \nu/\alpha && Sc = \nu/D \\
&\gamma = a/b && D_e = 4A/s.
\end{aligned} \tag{2}$$

Then the vorticity–velocity formulation of the governing equations can be obtained as [27]:

$$\xi = \partial U/\partial Y - \partial V/\partial X \tag{3}$$

$$\partial^2 U/\partial X^2 + \partial^2 U/\partial Y^2 = \partial\xi/\partial Y - \partial^2 W/\partial X\,\partial Z \tag{4}$$

$$\partial^2 V/\partial X^2 + \partial^2 V/\partial Y^2 = -\partial\xi/\partial X - \partial^2 W/\partial Y\,\partial Z \tag{5}$$

$$\begin{aligned}
&U\,\partial\xi/\partial X + V\partial\xi/\partial Y + W\partial\xi/\partial Z + \xi(\partial U/\partial X + \partial V/\partial Y) \\
&\quad + (\partial W/\partial Y\cdot\partial U/\partial Z - \partial W/\partial X\cdot\partial V/\partial Z) = \partial^2\xi/\partial X^2 \\
&\quad + \partial^2\xi/\partial Y^2 - (Ra\cdot\cos\delta/Pr)\cdot(\partial\theta/\partial X + N\cdot\partial C/\partial X)
\end{aligned} \tag{6}$$

$$\begin{aligned}
&U\partial W/\partial X + V\partial W/\partial Y + W\partial W/\partial Z = -\mathrm{d}\bar{P}/\mathrm{d}Z \\
&\quad + \partial^2 W/\partial X^2 + \partial^2 W/\partial Y^2 + (\Omega/Pr)\cdot(\theta + NC)
\end{aligned} \tag{7}$$

$$\begin{aligned}
&U\partial\theta/\partial X + V\partial\theta/\partial Y + W\partial\theta/\partial Z \\
&\quad = (\partial^2\theta/\partial X^2 + \partial^2\theta/\partial Y^2)/Pr
\end{aligned} \tag{8}$$

$$\begin{aligned}
&U\partial C/\partial X + V\partial C/\partial Y + W\partial C/\partial Z \\
&\quad = (\partial^2 W/\partial X^2 + \partial^2 W/\partial Y^2)/Sc.
\end{aligned} \tag{9}$$

An additional constraint which is used to deduce the axial pressure gradient in axial momentum equation is that global mass conservation at any axial location must be satisfied. This constraint could be expressed as

$$\int_0^{(1+\gamma)/(2\gamma)}\int_0^{(1+\gamma)/4} W\mathrm{d}X\mathrm{d}Y = (1+\gamma)^2/(8\gamma). \tag{10}$$

Because of the symmetry characteristics shown in Fig. 1, the boundary conditions could be given as:

$$U = V = W = 0, \theta = C = 1 \text{ at the duct walls} \tag{11a}$$

$$U = \partial V/\partial X = \partial W/\partial X = \partial\theta/\partial X = \partial C/\partial X = 0$$
$$\text{at the symmetric plane } X = (1+\gamma)/4 \tag{11b}$$

$$W = 1, U = V = \xi = \theta = C = 0$$
$$\text{at the entrance } Z = 0. \tag{11c}$$

The interfacial velocity at the walls as a result of mass diffusion process will be neglected in the analysis for the situation in which the concentration level is low, as has been discussed in refs. [28, 29]. Thus, the governing equations contain six dimensionless parameters: Ω, Ra^*, N, γ, Pr, and Sc. As defined by equation (2), Ω is a mixed convection parameter, i.e. the ratio of the Rayleigh number Ra to the Reynolds number Re, is modified by an inclination angle factor $\sin\delta$; $Ra^* = Ra\cos\delta$ is a modified Rayleigh number; the buoyancy ratio N represents the relative effect of chemical species diffusion on the thermal diffusion. When $N = 0$, the mass diffusion effect is negligible and the buoyancy force arises solely from the temperature difference. The buoyancy force from mass and thermal diffusion are combined to assist the flow when $N > 0$, whereas they oppose each other as $N < 0$.

It is seen that, with the introduction of the inde-

pendent parameters Ω and Ra^*, the inclination angle, δ, does not appear explicitly in the formulation. It is obvious that, for a horizontal rectangular duct [24];

$$\delta \to 0 : \sin\delta \to 0 \quad Ra^* \to Ra \quad \Omega \to 0 \tag{12}$$

while for a vertical duct [15, 22],

$$\delta \to \pi/2 : \sin\delta \to 1 \quad Ra^* \to 0 \quad \Omega \to Ra/Re \tag{13}$$

and the buoyancy term in the axial momentum equation (7) becomes

$$\delta \to \pi/2 : (\Omega/Pr)\cdot(\theta+NC) \to (Gr/Re)\cdot(\theta+NC). \tag{14}$$

Hence, the introduction of Ω and Ra^* as independent parameters has permitted a compact formulation, including the limiting cases of horizontal and vertical rectangular ducts.

The local friction factor, Nusselt number and Sherwood number are of practical interest, and could be calculated out from the velocity, temperature and concentration fields. Following the usual definitions, the expression for the product of the peripherally averaged friction factor and Reynolds number, fRe, can be written based on the axial velocity gradient at the walls,

$$fRe/(fRe)_0 = \overline{(\partial W/\partial n)}/\overline{(\partial W/\partial n)}_0. \tag{15}$$

The peripherally averaged Nusselt number Nu and Sherwood number Sh can be written based on the temperature and concentration gradients at the walls, respectively,

$$Nu = \overline{(\partial\theta/\partial n)}/(1-\theta_b) \tag{16}$$

$$Sh = \overline{(\partial C/\partial n)}/(1-C_b) \tag{17}$$

where the overbar in equations (15)–(17) represents average around the perimeter. The bulk fluid temperature θ_b and concentration C_b are evaluated as follows:

$$\theta_b = \int_0^{(1+\gamma)/(2\gamma)}\int_0^{(1+\gamma)/4} W\theta \,dX\,dY/(1+\gamma)^2/(8\gamma) \tag{18}$$

$$C_b = \int_0^{(1+\gamma)/(2\gamma)}\int_0^{(1+\gamma)/4} WC \,dX\,dY/(1+\gamma)^2/(8\gamma). \tag{19}$$

In this work, the results are presented for air ($Pr = 0.7$) over a Schmidt number range of 0.2–2.0. This covers diffusion into air of hydrogen ($Sc = 0.22$), water vapor (0.6), ethanol vapor (1.3) and benzene vapor (2.01) [28, 29]. Ω was varied between 0 and 200 and Ra^* was taken between 0 and 10^5. The buoyancy ratio N was varied between -0.8 and 2.0 with aspect ratios 0.2, 0.5, 1, 2 and 5.

METHOD FOR NUMERICAL SOLUTION

The governing equations are solved numerically by the vorticity–velocity method for three-dimensional parabolic flow [27]. The equations for the unknowns U, V, W, ξ, θ, C and $d\bar{P}/dZ$ are coupled. A marching technique based on the Du Fort–Frankel scheme [30] is developed for the solution of equations (4)–(9). For given values of Ω, Ra^*, N, Sc, γ and Pr, the numerical solution procedure for solving the unknown U, V, W, ξ, θ and C is briefly described below:

(1) Specify the initial values of U, V, W, ξ, θ and C, and guess a value of the axial pressure gradient $(d\bar{P}/dZ)$.

(2) For any axial location, with the known values of U, V and guessed $(d\bar{P}/dZ)$, the axial velocity W is obtained from equation (7) with the constraint of global continuity (10) to meet the requirement of constant flow rate. If the criterion

$$\left|\int_0^{(1\gamma)/(2\gamma)}\int_0^{(1+\gamma)/4} W\,dX\,dY-(1+\gamma)^2/(8\gamma)\right| < 10^{-6} \tag{20}$$

is satisfied, then the values of $\partial W/\partial X$ and $\partial W/\partial Y$ can be evaluated at each grid point.

(3) The values of $\partial U/\partial Z$ and $\partial V/\partial Z$ are computed using a two-point backward difference formula. With the known values of U, V and W, the new values of ξ, θ and C at the interior points of the next axial position are obtained from eqns (6), (8) and (9), respectively, by the Du Fort–Frankel method [30].

(4) The values of $\partial^2 W/\partial X\,\partial Z$, $\partial^2 W/\partial Y\,\partial Z$, $\partial\xi/\partial Y$ and $\partial\xi/\partial X$ in equations (4) and (5) are calculated by using the backward difference axially and a central difference in the transverse directions. The elliptic-type equations (4) and (5) are then solved for U and V by an iteration process. During the iteration process, values of vorticity on boundaries are evaluated simultaneously with U and V in the interior region. The boundary vorticity on the wall of $X = 0$ is [12]:

$$\xi_{1,j} = -\xi_{2,j}-2V_{2,j}/\Delta X+(U_{2,j+1}-U_{2,j-1})/(2\Delta Y). \tag{21}$$

It is noted that the boundary vorticities on the other walls can also be computed in a similar expression.

(5) Steps (2)–(4) are repeated at a cross section until the following criterion is satisfied for the velocity components U and V,

$$\varepsilon = \max|\phi_{i,j}^{m+1}-\phi_{i,j}^{m}|/\max|\phi_{i,j}^{m+1}| < 10^{-5} \qquad \phi = U \text{ or } V \tag{22}$$

where m is the mth iteration of steps (2)–(4).

(6) Steps (2)–(5) are repeated at each cross plane from the inlet to the downstream region of interest.

To ensure the independence of the numerical results, a numerical experiment was made on the grid lines $I\times J$ and axial step size ΔZ^*. The grid lines in the X and Y directions are uniform, while nonuniform

Table 1. Comparisons of local Nu and $(fRe)/(fRe)_0$ for various grid arrangements for $\Omega = 100$, $Ra^* = 5 \times 10^4$, $N = 1$, $Sc = 1.3$ and $\gamma = 1$

$I \times J$ (ΔZ^*)	0.002	0.005	0.01	Z^* 0.03	0.066	0.1	0.4
				Nu			
30×60 (1.0×10^{-5}–5.0×10^{-4})	10.05	7.45	6.91	7.35	6.10	5.20	3.08
20×40 (2.0×10^{-6}–5.0×10^{-4})	10.28	7.55	7.04	7.43	6.14	5.21	3.09
20×40 (1.0×10^{-5}–5.0×10^{-4})	10.25	7.54	7.04	7.43	6.14	5.21	3.09
10×20 (1.0×10^{-5}–5.0×10^{-4})	12.28	8.55	8.15	8.20	6.86	5.21	3.09
$I \times J$ (ΔZ^*)	0.002	0.005	0.01	Z 0.03	0.066	0.1	0.4
				$(fRe)/(fRe)_0$			
30×60 (1.0×10^{-5}–5.0×10^{-4})	2.99	2.79	2.75	2.05	1.49	1.35	1.03
20×40 (2.0×10^{-6}–5.0×10^{-4})	2.95	2.75	2.72	2.02	1.47	1.34	1.03
20×40 (1.0×10^{-5}–5.0×10^{-4})	2.95	2.75	2.72	2.02	1.48	1.34	1.03
10×20 (1.0×10^{-5}–5.0×10^{-4}	2.78	2.60	2.60	1.87	1.44	1.33	1.02

axial step size is employed to account for the uneven variations of W, θ and C at the region near the inlet. Table 1 presents the results of the local Nusselt number Nu and friction factor ratio $(fRe)/(fRe)_0$ for four arrangements of grid points in the x, y and z directions, respectively. It is found that the deviations in Nu and $(fRe)/(fRe)_0$ calculated with $I \times J = 20 \times 40$ and 30×60 ($\Delta Z^* = 1 \times 10^{-5} \sim 5 \times 10^{-4}$) are always less than 2%. Furthermore, the deviations in Nu and $(fRe)/(fRe)_0$ calculated using $I \times J$ (ΔZ^*) $= 20 \times 40$ ($2 \times 10^{-6} \sim 5 \times 10^{-4}$) and 20×40 ($1 \times 10^{-5} \sim 5 \times 10^{-4}$) are estimated to be within 1%. Thus, the computations involving an $I \times J$ (ΔZ^*) $= 20 \times 40$ (1×10^{-5}–5×10^{-4}) grid are considered to be sufficiently accurate to describe the heat and mass transfer in inclined rectangular ducts. In addition, the hydrodynamically developing flow was computed without buoyancy effects, and the results were compared with those of Shah and London [25]. The apparent friction factor was found to agree to within 2% at all axial locations. Besides, the limiting results of mixed convection heat transfer in horizontal ducts were also obtained and compared with those of Lin and Chou [14]; excellent agreement was found. All these confirm the accuracy and convergence of the present numerical solution.

RESULTS AND DISCUSSION

(A) *Developments of axial velocity, temperature and concentration profiles*

Although the presentation of the local friction factor, Nusselt number and Sherwood number in the simultaneously developing region is the major goal in this work, developments of axial velocity, temperature and concentration profiles are of engineering interest and useful in clarifying the heat and mass transfer mechanism. The developing profiles of the axial velocity W along the symmetric plane $X = 0.5$ are shown in Fig. 2. It is well known that the axial velocity profiles for purely forced convection without buoyancy effects are symmetric with respect to the $Y = 0.5$ line. Overall inspection on Fig. 2 reveals that, near the entrance, the velocity profile (curve A) is fairly uniform over the cross plane; as the flow moves downstream, the curves are distorted due to the buoyancy effects, and the nature of the distortion depends on the magnitude of Ω and Ra^*; at the farthest downstream location (curve F, $Z^* = 2.0$), the effects of buoyancy forces disappear and a fully-developed profile is attained. It is clear from the definition of Ω and Ra^* that the combination of a small Ω and a large Ra^* yields the case of mixed convection heat and mass transfer in a horizontal duct. In Fig. 2a, for $\Omega = 5$ and $Ra^* = 5 \times 10^4$, the velocity (curve A) is uniform and symmetric near the inlet; as the flow goes downstream, this symmetry is lost and the locations of the maximum axial velocity move toward the bottom wall due to the buoyancy-driven secondary flow. This is typical of mixed convection in a horizontal duct [12]. Figure 2b presents the developing W profiles for $\Omega = 100$ and $Ra^* = 5 \times 10^4$. In contrast to Fig. 2a, the maximum velocity is now displaced toward the top wall for curves C and D. This is because of the aiding buoyancy forces in the main flow direction with increasing value of Ω while keeping Ra^* fixed. Therefore, the W profiles are affected by both the cross-stream buoyancy and the aiding buoyancy forces in

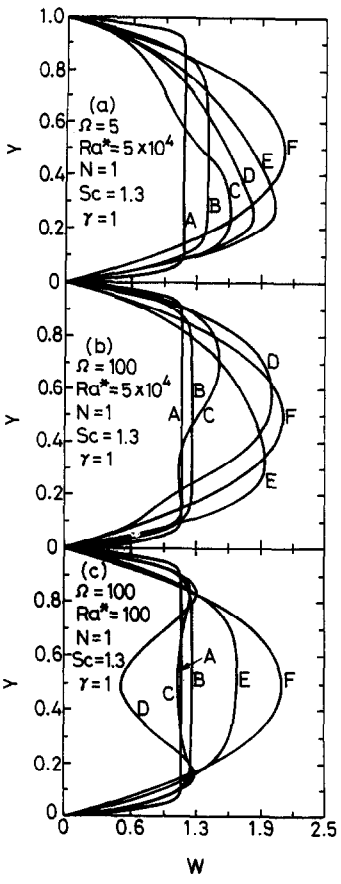

Fig. 2. Developments of axial velocity profiles for (a) $\Omega = 5$ and $Ra^* = 5 \times 10^4$; (b) $\Omega = 100$ and $Ra^* = 5 \times 10^4$; (c) $\Omega = 100$ and $Ra^* = 100$ with $N = 1$, $Sc = 1.3$ and $\gamma = 1$ (A: $Z^* = 0.0005$, B: $Z^* = 0.005$, C: $Z^* = 0.015$, D: $Z^* = 0.05$, E: $Z^* = 0.2$).

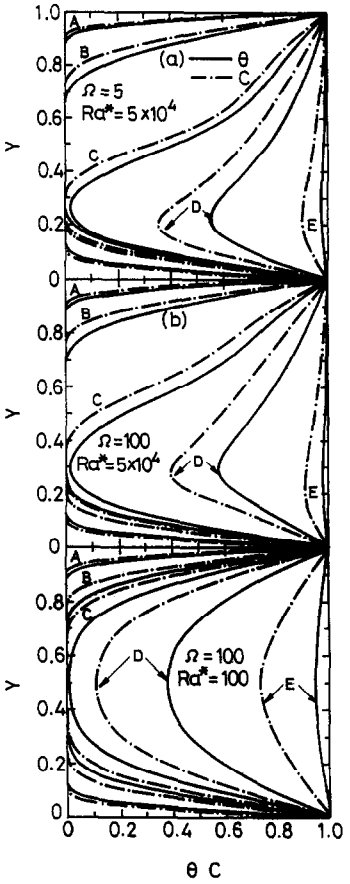

Fig. 3. Developments of axial temperature and concentration profiles for (a) $\Omega = 5$ and $Ra^* = 5 \times 10^4$; (b) $\Omega = 100$ and $Ra^* = 5 \times 10^4$; (c) $\Omega = 100$ and $Ra^* = 100$ with $N = 1$, $Sc = 1.3$ and $\gamma = 1$ (A: $Z^* = 0.0005$, B: $Z^* = 0.005$, C: $Z^* = 0.015$, D: $Z^* = 0.05$, E: $Z^* = 0.2$).

the axial direction. The W profiles for $\Omega = 100$ and $Ra^* = 100$ are shown in Fig. 2c. According to the definition of Ω and Ra^*, this combination of Ω and Ra^* yields the case of mixed convection heat and mass transfer in a vertical duct. Thus, the developing W profiles in Fig. 2c show no influence of cross-stream buoyancy forces and the curves are symmetric about the $Y = 0.5$ line. The W profile (curves C and D) is accelerated near the heated walls due to the greater buoyancy forces in the main flow direction.

The developments of temperature and concentration profiles are of interest in understanding the characteristics of heat and mass transfer. Figure 3 shows the developments of dimensionless temperature and concentration profiles. It is interesting to observe that both θ and C develop in a very similar fashion, but the temperature boundary layers develop a little more rapidly than the concentration boundary layers due to Pr ($=0.7$) being smaller than Sc ($=1.3$). An overall inspection of Fig. 3a discloses that the normal temperature and concentration gradients at the bottom wall are greater than those at the top wall and the minimum value for θ or C at each curve is located near the bottom wall. The locations of minimum θ or C shift toward the top wall as the value of Ω is increased, as is clearly seen in Fig. 3b. In Fig. 3c, due to the case of $\Omega = 100$ and $Ra^* = 100$ being the mixed convection heat and mass transfer in a horizontal duct, the θ and C profiles are symmetric with respect to the line $Y = 0.5$.

(B) Axial variations of local friction factor, Nusselt number and Sherwood number

The effects of mixed convection parameter Ω on the axial variations of $fRe/(fRe)_0$ at $Ra^* = 5 \times 10^4$, $N = 1$, $Sc = 1.3$ and $\gamma = 1$ are presented in Fig. 4. For clear illustration, the results near the inlet are specifically plotted in the inset in Fig. 4. The purely forced convection curve, denoted by E in Fig. 4, has been obtained by setting Ω and Ra^* to zero. Near the entrance, the buoyancy effects are insignificant and all the curves follow the forced convection curve. As the flow moves downstream, the buoyancy effects become important and each curve of the friction factor ratio branches out from the curve of forced convection (curve E). The buoyancy effects are the most pro-

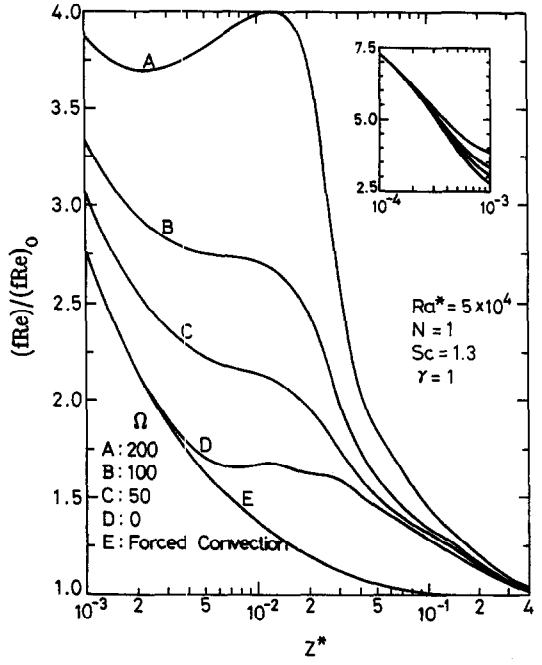

Fig. 4. The axial variations of the local friction factor ratio for $Ra^* = 5 \times 10^4$, $N = 1$, $Sc = 1.3$ and $\gamma = 1$ with Ω as parameter.

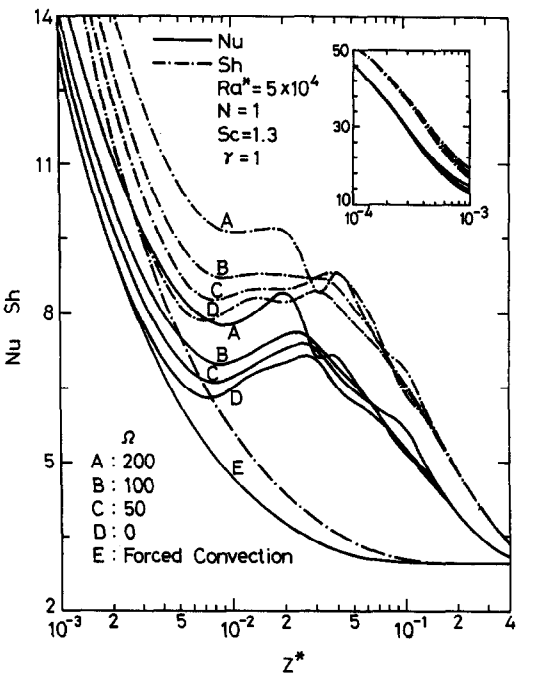

Fig. 5. The axial variations of the local Nusselt and Sherwood numbers for $Ra^* = 5 \times 10^4$, $N = 1$, $Sc = 1.3$ and $\gamma = 1$ with Ω as parameter.

nounced at the highest value of Ω, since this parameter represents a ratio of natural convection to forced convection effects. At $\Omega = 200$, the maximum value of $fRe/(fRe)_0$ occurs at approximately $Z^* = 1.23 \times 10^{-2}$. The occurrence of maximum local friction factor is closely related to the appearance of local maximum secondary flow intensity [14]. Finally, the curves decrease asymptotically to the line of $fRe/(fRe)_0 = 1$ when the velocity profile becomes fully developed.

The axial variations of *Nu* and *Sh* for different values of Ω are shown in Fig. 5, with the results near the entrance plotted in the inset. The decrease of Nusselt (Sherwood) number near the inlet is known to be the forced-convection entrance effect, and the deviation from the forced convection result is due to the buoyancy effects. It is clear that the entrance and buoyancy effects will eventually balance out and the local minimum *Nu* (*Sh*) number appears at a specific distance from the inlet, which depends on the value of Ω. Subsequently, the buoyancy effect dominates over the entrance effect and the *Nu* (*Sh*) increases until the local minimum value for *Nu* (*Sh*) is reached. After reaching the first minimum in *Nu* (*Sh*), maximum and minimum local *Nu* (*Sh*) may exist for some cases. Finally, the curves of *Nu* (*Sh*) lower asymptotically the value of Graetz solution when the temperature (concentration) profiles become fully developed. The first minimum in the *Nu* (*Sh*) and the subsequent maximum and minimum are also found in the results of mixed convection heat transfer in a horizontal duct [10] and a horizontal tube [13]. In addition, it is found that the value of *Sh* is larger than that of *Nu*. This is due to the fact that the Schmidt number ($Sc = 1.3$) is larger than the Prandtl number ($Pr = 0.7$) in the flow system.

Figure 6 shows the axial variations of Nu and Sh for different modified Rayleigh number Ra^* at $\Omega = 100$,

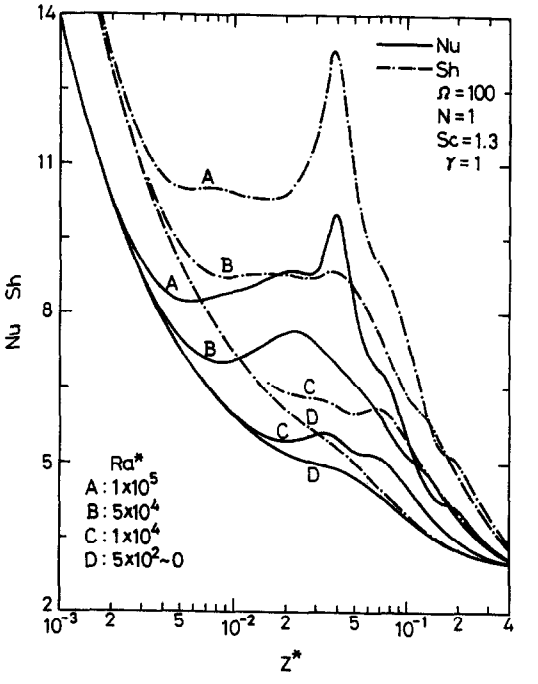

Fig. 6. The axial variations of the local Nusselt and Sherwood numbers for $\Omega = 100$, $N = 1$, $Sc = 1.3$ and $\gamma = 1$ with Ra^* as parameter.

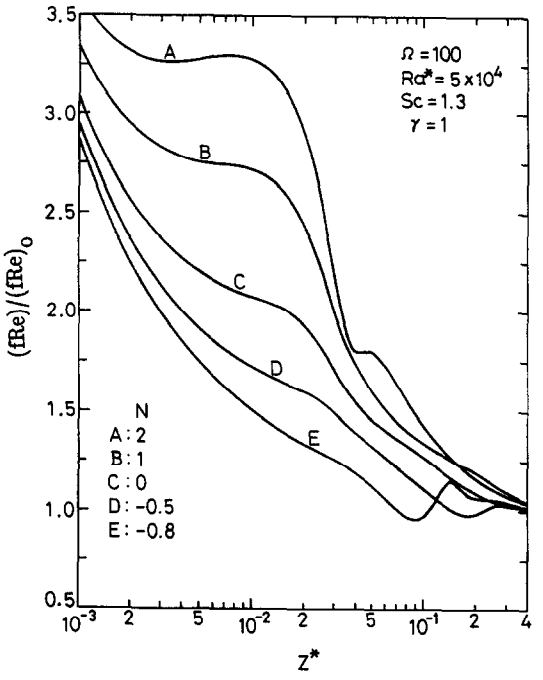

Fig. 7. The axial variations of the local friction factor ratio for $\Omega = 100$, $Ra^* = 5 \times 10^4$, $Sc = 1.3$ and $\gamma = 1$ with N as parameter.

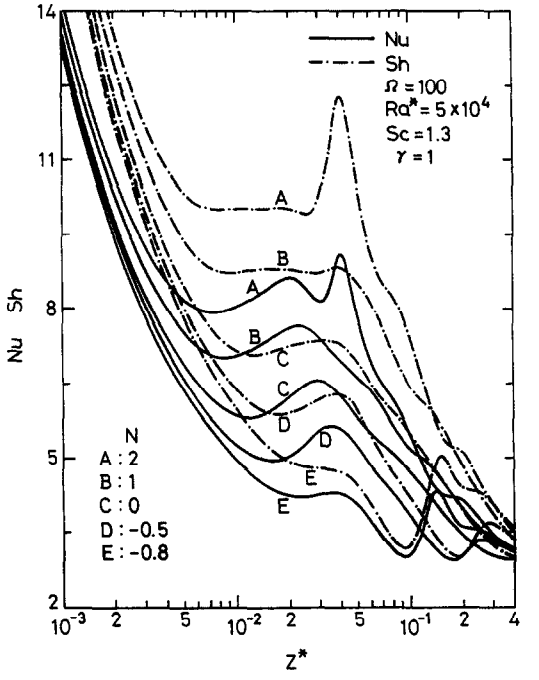

Fig. 8. The axial variations of the local Nusselt and Sherwood numbers for $\Omega = 100$, $Ra^* = 5 \times 10^4$, $Sc = 1.3$ and $\gamma = 1$ with N as parameter.

$N = 1$, $Sc = 1.3$ and $\gamma = 1$. From the defining equations of Ra^* and Ω, equation (2), it is seen that holding Ω fixed while increasing Ra^* is like decreasing the inclination angle δ and simultaneously increasing the Rayleigh number Ra. Alternatively, the same effect can be obtained at a fixed inclination angle δ by increasing Ra and Re simultaneously such that the value of Ω remains the same. In any case, the effect of increasing Ra^* at a fixed Ω is to increase the combined buoyancy effects. As shown in Fig. 6, the effect of Ra^* is practically negligible when $Ra^* \leqslant 5 \times 10^2$. A monotonic decrease of Nu (Sh) near the inlet is caused by the entrance effect. The onset of buoyancy effect occurs at some axial location from the inlet, depending mainly upon the value of Ra^*. A minimum local Nu (Sh) will not appear unless the entrance effect is balanced out by the buoyancy effects. After reaching the local minimum point, the variation of local Nu (Sh) generally shows an increase to a maximum local Nu (Sh). Peak value of local Nusselt (Sherwood) number for $Ra^* = 1 \times 10^5$ is noted. This is caused by the appearance of the second pair of eddies. At large downstream distance, the local Nu (Sh) gradually approaches the asymptotic value given by the Graetz solution when the temperature (concentration) profile becomes fully developed.

The variations of local $fRe/(fRe)_0$, Nu and Sh are presented in Figs. 7 and 8 with buoyancy ratio N as a parameter. As compared to the case of $N = 0$ (i.e. the case in which there is no mass buoyancy effect and the buoyancy force arises solely from the thermal variations), the local friction factor, Nusselt number and Sherwood number increase when the buoyancy force from species diffusion acts in the same direction as the thermal buoyancy force (i.e. $N > 0$), and the extent of the enhancement increases with N. For the cases of $N < 0$, the local $(fRe)/(fRe)_0$, Nu and Sh decrease with the increase in $|N|$ near the entrance. But in the downstream region, a local minimum and maximum Nu (Sh) appears in the curves of $N = -0.5$ and -0.8. Inspection of Figs. 7 and 8 further indicates that the location at which enhancement begins advances upstream with increasing N. This effect is due to the increase in the combined buoyancy effects of thermal and solutal diffusion.

Figure 9 gives the effects of Schmidt number on the Nusselt and Sherwood numbers. It is clearly seen that the effects of Sc on the local Nu is insignificant. But the influence of Sc on the local Sh is considerable. The results of Fig. 9(b) indicate that, for a given Ω, Ra^*, N and γ, a larger Sh is experienced for a system with a larger Sc. That is, the mass transfer rate increases with the increase in Schmidt number. This is due to the fact that a larger Schmidt number corresponds to a smaller binary diffusion coefficient for a given mixture and to a thinner concentration boundary-layer thickness relative to the flow boundary-layer thickness. This results in a larger mass transfer rate at the duct wall or a larger Sh number.

The effect of the aspect ratio of a rectangular duct on the heat transfer results is of practical interest. The local Nu for the aspect ratios $\gamma = 2$ and 0.5 is shown in Fig. 10 with mixed convection parameter Ω as parameter. In Fig. 10, the lowest curve can be regarded

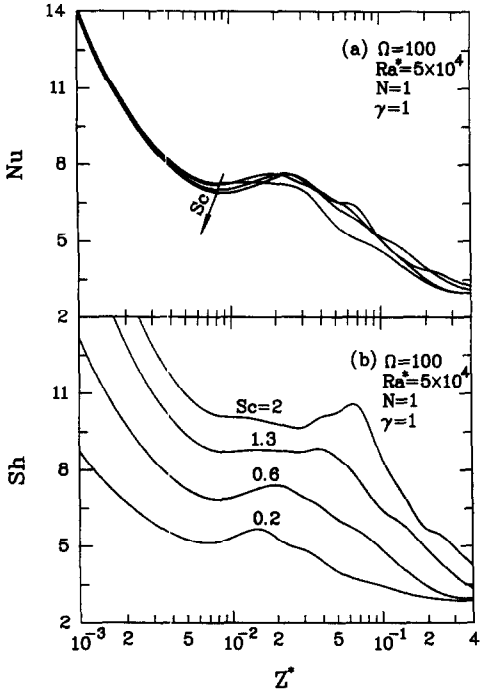

Fig. 9. The axial variations of the local Nusselt and Sherwood numbers for $\Omega = 100$, $Ra^* = 5 \times 10^4$, $N = 1$ and $\gamma = 1$ with Sc as parameter.

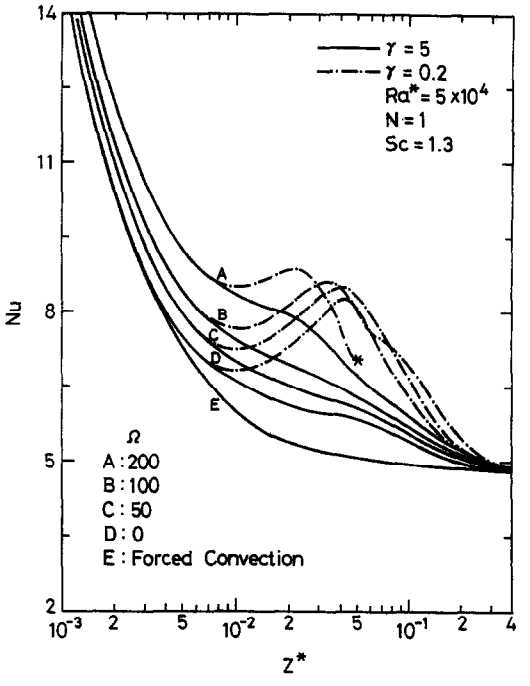

Fig. 11. The axial variations of the local Nusselt number with Ω as parameter for $\gamma = 5$ and 0.2.

as a limiting case for purely forced convection. Comparing Figs. 5 and 10, it is found that the general behaviors of the Nu for aspect ratios $\gamma = 2$ and 0.5 are quite similar to those of $\gamma = 1$. However, the results show that the aspect ratio $\gamma = 0.5$ (narrow and tall channel) is superior to $\gamma = 2$ (thin and flat channel). This is because that the relatively longer vertical side wall has a stronger buoyancy effect on the flow, heat and mass transfer for a channel with a smaller γ. Similar results are also found in Fig. 11 for the results of local Nu for $\gamma = 5$ and 0.2. It is worth noting that the symbol * in curve A represents the location of flow reversal.

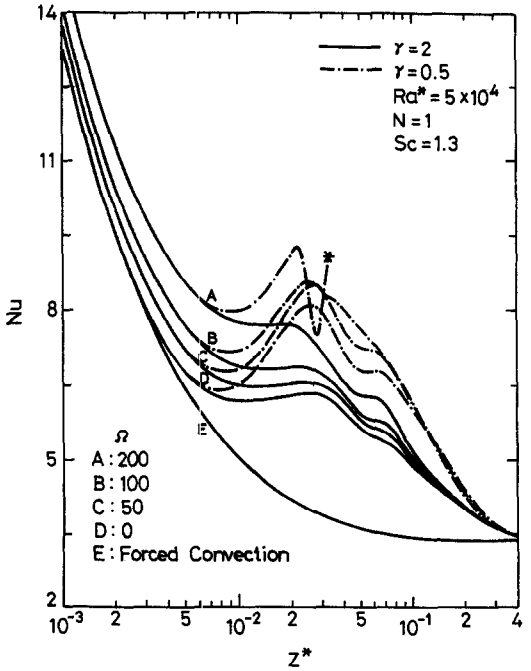

Fig. 10. The axial variations of the local Nusselt number with Ω as parameter for $\gamma = 2$ and 0.5.

CONCLUSION

The transport phenomena of developing laminar mixed convection heat and mass transfer in inclined rectangular ducts have been solved using a vorticity–velocity method. The effects of the mixed convection parameter Ω, modified Rayleigh number Ra^*, buoyancy ratio N, Schmidt number Sc and aspect ratio γ on the momentum, heat and mass transfer were examined in detail. The major results could be summarized as below:

(1) The buoyancy forces distort the axial velocity, temperature and concentration distributions and the nature of the distortion depends on the relative magnitudes of Ω and Ra^*.

(2) For the range of parameters under investigation, the buoyancy effects are practically negligible only when $Ra^* \leqslant 5 \times 10^2$.

(3) The variations of the local Nusselt (Sherwood) number are characterized by a decay near the inlet in which the forced-convection entrance effect dominates, but the decay is attenuated by the onset of buoyancy-driven secondary flows and the aiding of buoyancy forces in the main flow direction. After a

first local minimum is reached, maximum and minimum local *Nu* (*Sh*) may exist for some cases. Finally, the *Nu* (*Sh*) falls asymptotically to the value of Graetz problem when the temperature (concentration) profile becomes fully developed.

(4) A larger *Sh* is experienced for a system with a larger *Sc*.

Acknowledgement—The financial support of this research by the National Science Council under the contract NSC 82-0401-E211-003 is greatly appreciated.

REFERENCES

1. K. C. Cheng and G. J. Hwang, Numerical solution for combined free and forced laminar convection in horizontal rectangular channels, *J. Heat Transfer* **91,** 59–66 (1969).
2. H. Nakamura, A. Matsura, J. Kiwaki, S. Hiraoka and J. Yamada, Numerical solutions for combined free and forced laminar convection in horizontal rectangular ducts by conjugate gradient method, *J. Chem. Engng* **11,** 354–360 (1978).
3. M. Iqbal and J. W. Stachiewicz, Influence of tube orientation on combined free and forced laminar convection heat transfer, *J. Heat Transfer* **88,** 109–116 (1966).
4. K. C. Cheng and S. W. Hong, Effect of tube inclination on laminar convection in uniformly heated tubes for flat-plate solar collectors, *Solar Energy* **13,** 363–371 (1972).
5. J. W. Ou, K. C. Cheng and R. C. Lin, Combined free and forced laminar convection in inclined rectangular channels, *Int. J. Heat Mass Transfer* **19,** 277–283 (1976).
6. J. A. Sabbagh, A. Aziz, A. S. El-Aring and G. Hamad, Combined free and forced convection heat transfer in inclined circular tubes, *J. Heat Transfer* **98,** 322–324 (1976).
7. A. M. Abdelmeguid and D. B. Spalding, Turbulent flow and heat transfer in pipes with buoyancy effects, *J. Fluid Mech.* **94,** Part 2, 383–400 (1979).
8. M. M. M. Abou-Ellail and S. M. Morcos, Buoyancy effects in the entrance region of horizontal rectangular chennels, *J. Heat Transfer* **105,** 924–928 (1983).
9. F. P. Incropera and J. A. Schutt, Numerical simulation of laminar mixed convection in the entrance region of horizontal rectangular ducts, *Numer. Heat Transfer* **8,** 707–729 (1985).
10. H. V. Mahaney, F. P. Incropera and S. Ramadhyani, Development of laminar mixed convection flow in a horizontal rectangular duct with uniform bottom heating, *Numer. Heat Transfer* **12,** 137–155 (1987).
11. F. P. Incropera, A. L. Knox and J. R. Maughan, Effect of wall heat flux distribution on laminar mixed convection in the entry region of a horizontal rectangular duct, *Numer. Heat Transfer* **13,** 427–450 (1988).
12. F. C. Chou and G. J. Hwang, Vorticity–velocity method for Graetz problem with the effect of natural convection in a horizontal rectangular channel with uniform wall heat flux, *J. Heat Transfer* **109,** 704–710 (1987).
13. F. C. Chou and G. J. Hwang, Numerical analysis of the Graetz problem with natural convection in a uniformly heated horizontal tube, *Int. J. Heat Mass Transfer* **31,** 1299–1308 (1988).
14. J. N. Lin and F. C. Chou, Laminar mixed convection in the thermal entrance region of horizontal isothermal rectangular channels, *Can. J. Chem. Engng* **67,** 361–367 (1989).
15. C. H. Cheng and C. J. Weng, Developing flow of mixed convection in a vertical rectangular duct with one heating wall, *Numer. Heat Transfer* **24,** Part A, 479–493 (1993).
16. M. M. M. Abou-Ellail and S. M. Morcos, Combined forced and free laminar convection in the entrance region of inclined rectangular channels, *Proc. Int. Conf. Numerical Methods for Non-Linear Problems* (Edited by C. Taylor *et al.*), pp. 807–821. Pineridge Press, Swansea (1980).
17. E. M. Morcos and M. M. M. Abou-Ellail, Buoyancy effects in the entrance region of an inclined multi-rectangular channel solar collector, *ASME J. Solar Energy Engng* **105,** 157–162 (1983).
18. K. C. Cheng and F. P. Yuen, Flow visualization studies on secondary flow pattern for mixed convection in the entrance region of isothermally heated inclined pipes. In *Fundamentals of Forced and Mixed Convection*, HTD-Vol. 42, pp. 121–130. ASME, New York (1985).
19. S. M. Morcos, M. M. Hilal, M. M. Kamel and M. S. Soliman, Experimental investigation of mixed laminar convection in the entrance region of inclined rectangular channels, *J. Heat Transfer* **108,** 574–579 (1986).
20. D. Choudhury and S. V. Patankar, Combined forced and free laminar convection in the entrance region of an inclined isothermal tube, *J. Heat Transfer* **110,** 901–909 (1988).
21. F. Santarelli and F. P. Foraboschi, Heat transfer in laminar mixed convection in a reacting fluid, *Chem. Engng* **6,** 59–68 (1973).
22. W. M. Yan, Mixed convection heat transfer enhancement through latent heat transport in vertical parallel plate channel flows, *Can. J. Chem. Engng* **69,** 1277–1282 (1991).
23. W. M. Yan, Effects of film evaporation on laminar mixed convection heat and mass transfer in a vertical channel, *Int. J. Heat Mass Transfer* **35,** 3419–3429 (1992).
24. J. N. Lin, F. C. Chou, W. M. Yan and P. Y. Tzeng, Combined buoyancy effects of thermal and mass diffusion on laminar forced convection in the thermal entrance region of horizontal square channels, *Can. J. Chem. Engng* **79,** 681–689 (1992).
25. R. A. Shah and A. L. London, Laminar flow forced convection in ducts, *Adv. Heat Transfer* Suppl. 1, 196–222 (1978).
26. S. V. Patankar and D. B. Spalding, A calculation procedure for heat, mass and momentum transfer in three-dimensional parabolic flows, *Int. J. Heat Mass Transfer* **15,** 1784–1806 (1972).
27. K. Ramakrishna, S. G. Rubin and P. K. Khosla, Laminar natural convection along vertical square ducts, *Numer. Heat Transfer* **5,** 59–79 (1982).
28. B. Gebhart and L. Pera, The nature of vertical natural convection flows resulting from the combined buoyancy effects of thermal and mass diffusion, *Int. J. Heat Mass Transfer* **14,** 2025–2050 (1971).
29. T. S. Chen and C. F. Yuh, Combined heat and mass transfer in natural convection along a vertical cylinder, *Int. J. Heat Mass Transfer* **23,** 451–461 (1980).
30. P. J. Roache, *Computational Fluid Dynamics*, pp. 61–64. Reinhold, New York (1971).